Aerodynamic Investigations on Inclined Airship Bodies

Th. Lutz, P. Funk, A. Jakobi, S. Wagner
Institut für Aerodynamik und Gasdynamik
Universität Stuttgart
Pfaffenwaldring 21
D-70550 Stuttgart
Germany

Phone : +49 711 685 3409
Fax : +49 711 685 3438
Email : {lutz,funk,ajakobi,wagner}@iag.uni-stuttgart.de

Abstract

Theoretical and experimental investigations concerning the viscous flow about airship bodies will be presented. Special emphasis is laid on the aerodynamics at high angles of attack or sideslip, where complex three-dimensional boundary-layer separation occurs. The flow separation has a decisive influence on the pressure distribution as well as on the load and moment distribution. The determination of the three-dimensional separation line is therefore of great importance. It will be shown that the separation line can be derived by means of three-dimensional boundary-layer computations without using empirical criteria. Calculations for the contour of the solar-powered airship 'Lotte' will be presented and compared with wind and water tunnel test results.

Nomenclature

$c_{LV} = \frac{L}{\frac{\rho_\infty}{2} U_\infty^2 \cdot V^{2/3}}$	volumetric lift coefficient
$c_{DV} = \frac{D}{\frac{\rho_\infty}{2} U_\infty^2 \cdot V^{2/3}}$	volumetric drag coefficient
$c_{MV} = \frac{M}{\frac{\rho_\infty}{2} U_\infty^2 \cdot V}$	volumetric pitching moment coefficient
D	drag
L	body length, lift
M	pitching moment
$Re_L = \frac{U_\infty \cdot L}{\nu}$	Reynolds number based on body length L
s/L	dimensionless arc length

Tu	turbulence level
U_∞	onset flow velocity
V	body volume
x/L	dimensionless x-coordinate
x_{tra}/L	dimensionless transition point location
y/L	dimensionless y-coordinate
α	angle of attack
β	angle of sideslip
ν	kinematic viscosity
ρ_∞	onset flow density
τ_W	skin friction
Ψ	circumferential angle

1 Introduction

Lighter-than-air flight is characterized by the fact that the required lift is obtained by the buoyancy of the hull. The generation of static lift enables to hover or to fly at low speeds. During manoeuvres or in gusty conditions high angles of attack or sideslip can occur. This results in complex three-dimensional flow separation. The separating shear layer causes aerodynamic forces on the blunt airship body, which depend non-linear on angle of attack. The resulting moment is unstable for usual airship configurations. For this reason, flight mechanics is very important for the design of airships. Because of the non-linear force and moment curves, the equations of motion cannot be solved analytically. Numerical flight simulations have to be carried out, therefore, aerodynamic data for all occuring flight conditions is required.

In order to efficiently determine the aerodynamic forces and moments, mostly empirical or semi-empirical computation methods are applied (see for example [2], [3] or [9]). The models are supplemented and improved on the basis of experimental data obtained from wind tunnel and flight tests. An exact calculation of the flow conditions, for example the pressure distribution, the boundary-layer development or the separation lines cannot be performed with these simplified methods. The computation of complex flow details requires moreover the application of numerical methods based on the solution of Reynolds-averaged Navier-Stokes equations. These CFD procedures still show problems in case of large separated flow regimes and also require an enormous amount of computation time. An application for the generation of an aerodynamic data base for a large number of different onset flow conditions is at this time out of question.

Therefore, simplified physical models are required to enable an efficient calculation of the flow about airship configurations. Primarily, methods based on potential theory are used which have to be coupled with a boundary-layer procedure in order to account for viscous effects (see for example [14]). Such methods were applied at our institute for aerodynamic investigations on airship bodies and were refined by implementation of a wake model [4], [5]. Within the framework of a research project at the University of Stuttgart, improved 3D-boundary-layer methods are being developed which should enable a more generally valid calculation. Accompanying experimental investigations in wind and water tunnels give insight into the flow phenomena occuring with inclined airship bodies, especially on the topology of three-dimensional separation. Additionally, a data base for the validation of the theoretical calculation methods will be compiled. The paper presented gives an overview of preliminary studies and first results of the research project in process.

2 Flow Phenomena

In viscous flow about bodies, a boundary-layer is formed on the surface, in which the flow velocity rises continuously from zero at the wall up to the velocity of the outer flow. One has to distinguish between a laminar and a turbulent condition. A laminar boundary-layer is characterized by low skin friction. Because of the very large Reynolds number, however, no extensive laminar flow regions can be expected for conventional airship hulls. With an axial onset flow, the turbulent boundary-layer is usually attached up to the tail. The aerodynamic drag mainly results from skin friction forces. In the case of small Reynolds numbers and blunt tail geometries, a dead-air separation may appear which results in an additional pressure drag.

The flow about an inclined airship hull is three-dimensional, which means, that a pressure gradient transverse to the main direction of flow occurs. As a consequence, the streamlines at the boundary-layer edge are curved. The transverse pressure gradient causes the velocity vectors of the retarded fluid in the boundary-layer to turn. Fig. 2.1 illustrates the limiting streamlines for a model of an inclined airship body as an example.

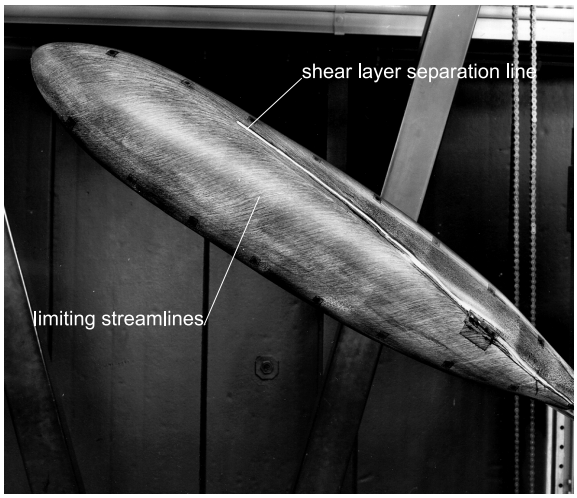

Fig. 2.1: Flow pattern of an inclined airship hull [11]
($\alpha = 30°$, $Re_L = 1.5 \cdot 10^6$)

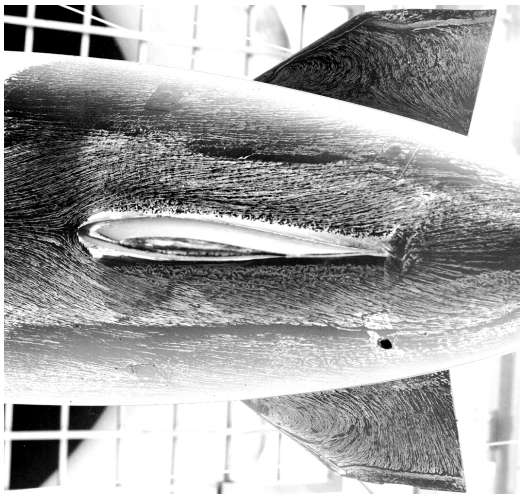

Fig. 2.2: Limiting streamlines on the suction side of a hull-fin combination [11]
($\alpha = 20°$, $Re_L = 1.5 \cdot 10^6$)

In the wind-tunnel test the limiting streamlines were visualised by means of the petroleum-soot method. This method gives a time-averaged picture of the real flow. The limiting streamlines converge into an envelope, which represents the three-dimensional separation line. From this open separation line a vortex layer detaches on both sides of the inclined body. Each shear layer rolls up into a single vortex similar to the tip vortex of a wing. The separation effects also occur with very high Reynolds numbers.

Due to the induction effect of the vortex layer the pressure distribution on the hull, especially at the suction side, is strongly affected. This causes dynamic lift and induced drag. Since the length of the three-dimensional separation-line depends on angle of attack, a non-linear behaviour of the forces and moments results. The bare hull shows an unstable aerodynamic moment up to very large angles of attack. By mounting fins in the tail region the unstable

moment can be reduced. With usual airship designs there remains a slight static instability at small angles of attack, which can, however, be controlled by the pilot.

A fin of an airship represents a wing with a small aspect ratio which is characterized by side edge separation of the flow. With large sweep angles additional leading edge separation can occur. As a further problem, strong interference effects between the airship hull and the fins complicate the aerodynamics and the calculation of the detailed flow field. Fig. 2.2 depicts the complex flow pattern on the suction side of an inclined hull-fin combination.

Furthermore, the flow field of a complete airship configuration is influenced by the propulsion system. In the case of a stern-mounted propeller the outer flow in the tail region of the hull is accelerated. This results in an additional pressure drag. On the other hand a stern propeller is working in the viscous wake of the body, where the axial velocity component is reduced. If the propeller is properly designed, this leads to reduced power required to produce a certain thrust [6].

With an unsteady motion of the airship additional aerodynamic forces arise, as not only the inert airship itself but also the surrounding fluid has to be accelerated. These unsteady aerodynamic forces range in the order of magnitude of the inertia forces if the mass of the configuration is in the same order as the displaced fluid mass, which is true for airships. Usually, the unsteady aerodynamic forces are considered according to the principle of virtual mass. The added mass represents a tensorial quantity, not a scalar one like the inert mass does. In the general three-dimensional case 21 independent added mass terms can be distinguished. In the following paragraphs only the steady flow about airships, in particular the bare hull, are considered.

3 Wind and Water Tunnel Tests on an Inclined Airship Body

Within the framework of a research project at the University of Stuttgart investigations on the aerodynamic of airships are carried out. Apart from theoretical calculation and experimental tests in wind and water tunnel, in-flight tests with the remote-controlled solar-powered airship 'Lotte' are also planned.

3.1 Measurement of Forces and Moments

In a wind tunnel of the institute [10] force and moment measurements on the hull of 'Lotte' were carried out. As mentioned in section 1, these quantities are required for flight simulation. The tunnel is of 'Göttinger' type with circular jet cross section and an open measuring section. For the present investigations, the biggest nozzle of 1.75 m in diameter was used, which enables a maximum onset flow velocity of $U_\infty = 24$ m/s. Exactly downstream of the nozzle a lattice was fitted, which increases the turbulence level from Tu = 0.01 to Tu = 0.06. This guarantees an almost fully turbulent flow about the airship.

The scale of the wind-tunnel model of 'Lotte' is 1:20, which results in a model length of L = 0.8 m. In order to guarantee a high accuracy of the contour, the master model was manufactured on a CNC machine. Two negative semi-moulds, in which the model was laminated, were fabricated using glass fiber laminates. The measuring model, which is also made of laminated glass fiber, is constructed in two parts and is fixed together using toggle bolts. Despite consisting of two halves, a stable, true to contour body with a fine finish was obtained.

The wind-tunnel model was suspended with wires to a six-component balance located above the measuring section. In order to keep the wires tensioned for all flow conditions and to prevent drifting of the model, it was filled with lead shot. The balance consists of several frames which are supported using cross springs in such a way that the total force and its moment is converted into three components perpendicular to each other. The load was measured by six indicators in the balance coordinate system and subsequently transformed into aerodynamical coordinates. In order to obtain stationary mean values, large integration periods were chosen. Fig. 3.1 shows the volumetric force and moment curves. The experiments were performed at the maximum flow velocity of the tunnel, which corresponds to $Re_L = 1.3 \cdot 10^6$ with regard to our model. Reference point of the moment is the centre of volume, which is identical to the front point of suspension. The non-linear character of the lift curve slope is clearly visible. Due to the high turbulence level of the oncoming flow, a high drag coefficient at zero lift results. The static instability of the bare hull (see section 2) arises from the positive slope of the c_{MV}-α-graph.

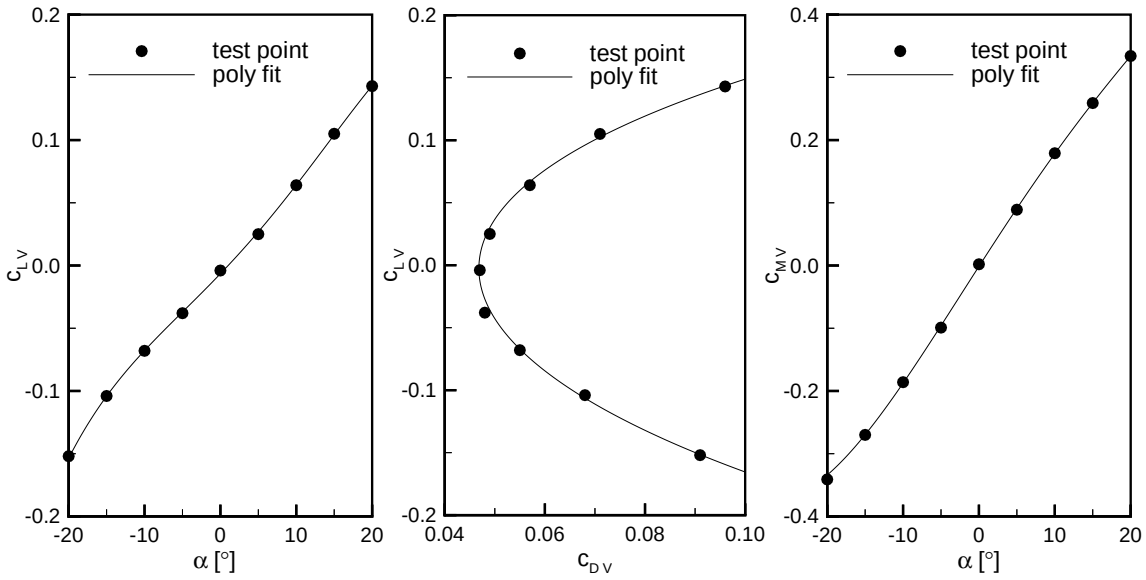

Fig. 3.1: Measured volumetric lift, drag and pitching moment coefficient for the hull of 'Lotte' ($Re_L = 1.3 \cdot 10^6$; Tu = 0.06)

3.2 Flow Visualisation

Flow visualisations were carried out in a water tunnel [15] of the institute in order to get an impression of the flow topology. Principally, flows which occur in air can be simulated in water, unless effects of compressibility have to be considered. Water tunnels are well suited for flow visualisations due to their kinematic viscosity, which is 15 times lower compared to air. Assuming equal overall dimensions and Reynolds numbers, processes in water pass 15 times slower than in air and can often be pursued with the naked eye. Naturally, the flow has to be marked properly. Beside this, the illuminating equipment is of extreme importance in flow visualisation.

For the experiments described below a model with a length of L = 0.60 m was CNC machined. A larger scale was not possible due to the blockage effect of the tunnel at higher angles of attack. The model is stern mounted in the tunnel. The rectangular measuring section is 2.84 m long, 1.52 m wide and 0.76 m high. The maximum flow velocity amounts to U_∞ = 2.5 m/s. The experiment chamber can be accessed from the top, it is vitrified both at the

side walls and at the ground. In order to avoid surface waves, a plexiglass pane covers the chamber during the experiments.

Surface Flow Patterns

Similar to the coatings with petroleum-soot (see Fig. 2.1), the limiting streamlines can also be marked in water. For this purpose the model is coated with a mixture of paraffin oil, oleic acid and titanium white. The optimal mixing ratio of these three components has to be adjusted to the wall shear stress and was determined to be 40 : 30 : 30 per cent by volume for the present investigations. In addition, it is of great importance how the coating is applied. Application with a foam roller produced best results, because it was possible to achieve a very thin and constant film. As a basic principle, there should result a state of equilibrium of the flow pattern quite soon after the tunnel was accelerated. In particular, this is an indication for the correct viscosity of the mixture.

The flow velocity of the tunnel was adjusted to $U_\infty = 1.7$ m/s, which corresponds to a Reynolds number of $Re_L = 1.0 \cdot 10^6$. Transition was forced by means of a turbulator at $x/L = 0.05$. Fig. 3.2 shows the flow pattern at $\alpha = 10°$, $\alpha = 20°$ and $\alpha = 30°$. There is a bright region at all angles of attack, where the wall shear stress is very low and consequently the coating cannot flow off. From the pressure side, the limiting streamlines converge towards this 3D-separation region. On the suction side, a dark region with high wall shear stress follows. The partition between these two regions is very striking. It can also be recognized that with increasing angle of attack the separation region extends towards the body nose.

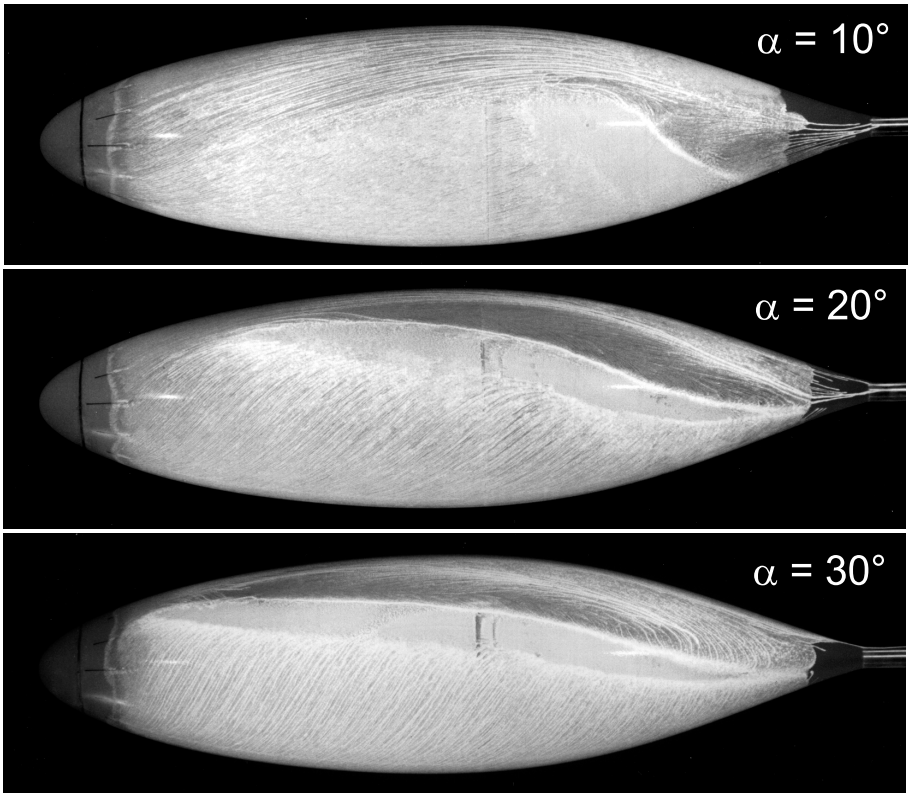

Fig. 3.2: Surface flow patterns at the inclined hull of 'Lotte'
($Re_L = 1.0 \cdot 10^6$; $x_{tra}/L = 0.05$; side view)

Hydrogen Bubble Method

In addition to the surface flow patterns, the flow was visualised by hydrogen bubbles. The method is based on the electrolysis of water. In electrolytes, the transport of charge results from ions, i.e. positively (cation) or negatively (anion) charged molecules. The conductivity of normal water is sufficient, so after applying a voltage to two electrodes, hydrogen and oxygen develop. If a thin wire of stainless steel is chosen as cathode, even the finest hydrogen bubbles can no longer adhere to the wire and are carried away by the flow. The diameter of the bubbles and that of the wire are of the same magnitude. The bubbles can be distinguished from a dark background, if they are illuminated at an angle of 120° in respect to the view direction by a lamp of high intensity (total reflection).

The static lift of the bubble at the ratio of viscosity which impedes the lifting increases with bubble size. This is the reason why the bubble diameter and consequently the diameter of the wire should be as small as possible. Due to the diffusion of bubbles, the hydrogen bubble method is restricted to small Reynolds numbers and slightly turbulent flows [8].

Fig. 3.3 shows a dead-air separation on an axially oriented hull, visualised by hydrogen bubbles. The wire is located in flow direction at the top of the model. Owing to the limitations described above, the experiments were performed at a Reynolds number of $Re_L = 0.3 \cdot 10^6$ and natural transition.

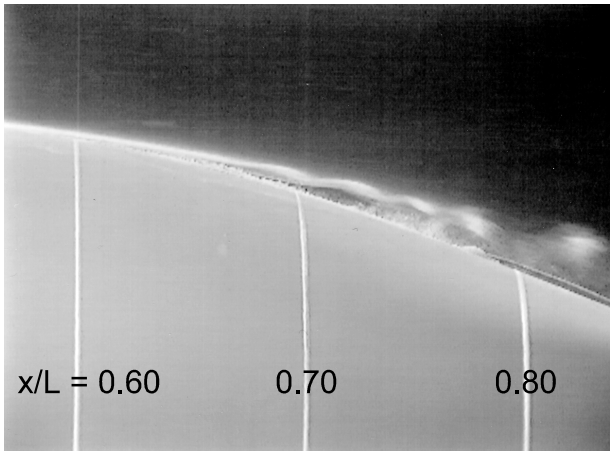

Fig. 3.3: Dead-air separation on the axially oriented hull of 'Lotte' ($Re_L = 0.3 \cdot 10^6$, natural transition)

4 Theoretical Investigations

4.1 Coupled Panel and Boundary-Layer Method

In order to carry out parametrical aerodynamical computations on inclined airship hulls a simplified calculation method was developed. A detailed description of the theoretical approach is given in [4] and [5] and is presented comprehensively hereafter.

For the calculation of the outer flow, a low-order 3D-panel method is employed which works with source singularities on the body surface. The unknown singularity distribution is determined by application of the external von Neumann boundary-condition at discrete collocation points. A boundary-layer calculation along inviscid streamlines is performed to

account for viscous effects. To that purpose, a first order 2D-integral method has been extended by inserting an additional term into the momentum and energy equations. This additional term represents the divergence of the inviscid streamlines and ensures satisfaction of the continuity equation in case of quasi-two-dimensional boundary-layers. Cross flow within the boundary layer is neglected with this simplified approach. For this reason, the calculation of the limiting streamlines and the theoretical determination of the shear-layer separation line is not possible.

For the approximate determination of the three-dimensional separation-line, an empirical criterion is applied, which was correlated on the basis of wind tunnel tests on an inclined airship body. The detaching free shear-layer is represented by a discrete number of free vortex filaments. With the present approach, the geometry of the wake is determined by means of a relaxation procedure which is based on the condition that the vortex filaments have to be force free.

The coupling of the panel-method, the boundary-layer procedure and the wake simulation is performed in an iterative way by means of a modification of the kinematic boundary condition. To achieve this, the velocity induced by the free shear-layers is superimposed to the onset flow vector at each panel control point. The displacement effect of the attached boundary layer and a possible dead-air region is considered by application of the transpiration technique.

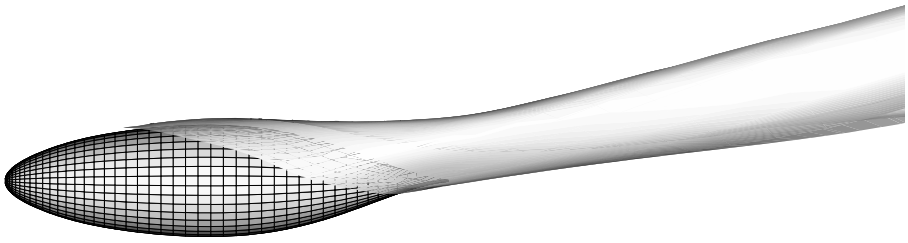

Fig. 4.1: Body shape and calculated wake geometry for the hull of 'Lotte' ($\alpha = 20°$, $Re_L = 1.0 \cdot 10^6$, $x_{tra}/L = 0.05$)

As a first example, calculation results for the inclined hull of 'Lotte' are presented. Fig. 4.1 shows the panel grid as well as the predicted wake geometry for an angle of attack of $\alpha = 20°$ and a Reynolds number of $Re_L = 1.0 \cdot 10^6$. The transition point was fixed at x/L = 0.05 as has been done in the water tunnel tests. Compared to the experimentally obtained separation line differences are obvious, which confirms the deficiencies of the applied empirical separation criterion. The calculated pressure distribution for the same onset-flow conditions is depicted as a contour plot in Fig. 4.2. Experimental data for comparison is not available yet.

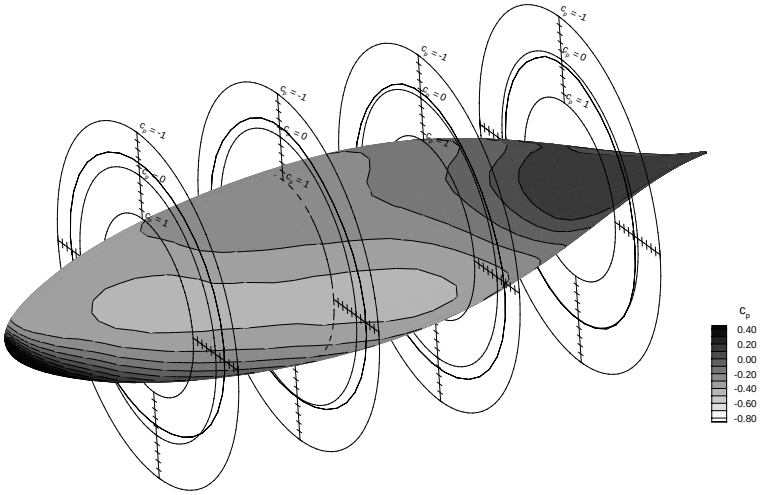

Fig. 4.2: Calculated pressure distribution for the hull of 'Lotte' ($\alpha = 20°$, $Re_L = 1.0 \cdot 10^6$, $x_{tra}/L = 0.05$)

In a further application of the calculation method, flow simulations for the projected heavy load airship CargoLifter were carried out. Fig. 4.3 shows the surface grid of the hull, which shows a slight heart-shaped cross section, caused by the elastic deformation of the envelope. The calculated and the measured lift curve slope of the bare hull are shown in Fig. 4.4 for $Re_L = 1.5 \cdot 10^6$. The non-linear character of the curve can be seen. The agreement between the theoretical and the experimental results is satisfactory. Deviations could be attributed especially to shortcomings of the empirical separation criterion.

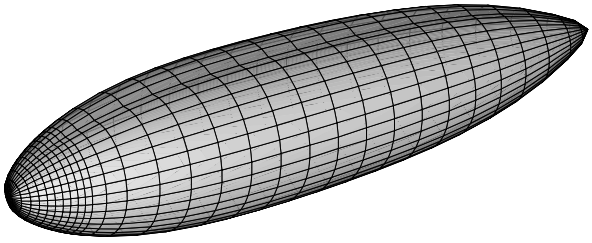

Fig. 4.3: Panel grid of the hull of CargoLifter

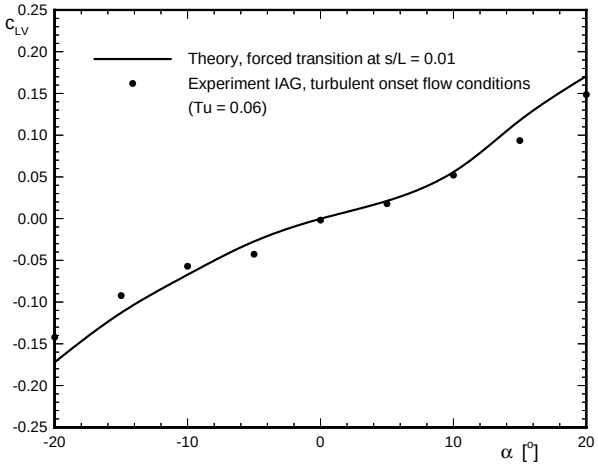

Fig. 4.4: Lift curve slope of the hull of CargoLifter ($\beta = 0°$, $Re_L = 1.5 \cdot 10^6$)

4.2 Three-Dimensional Boundary-Layer Calculation

In order to capture three-dimensional boundary-layer effects and to enable the calculation of the shear-layer separation-line a 3D-boundary-layer method is presently being developed at our institute.

The software INBOL solves the boundary-layer equations for laminar, three-dimensional flows [1]. The boundary-layer equations are implemented in form of the integral momentum equations and the second order 'Moment-of-Momentum'-equations [13]. The resulting system of ordinary differential equations is solved by means of the 'Method-of-Lines'.

It was already mentioned that the flow separation changes the pressure distribution on the airship body and the force and moment curves become non-linear. Furthermore, the assumptions of the basic equations are not valid in the region of separation and current methods abort the calculation when reaching this region. On the contrary, INBOL calculates on both sides of an open separation line. Therefore, it is possible to specify the boundary-layer development in the case of high angles of attack up to the end of the calculation grid, respectively up to the closed dead-air separation.

Validation of the Calculation Method

In order to validate the new method calculation results are compared to experimental data quantified by Meier/Kreplin [7]. Meier/Kreplin investigated in detail the flow field about an ellipsoid of revolution with a fineness ratio of 6:1. Their results are confirmed by several other experimental and theoretical investigations [12] and are therefore qualified for validation.

Fig. 4.5 shows the skin friction curves of the ellipsoid in circumferential direction at selected axial positions. The skin friction distributions are extracted from the forebody region for an angle of attack of $\alpha = 10°$. The flow conditions are still laminar in this part of the body so the calculation results can be directly compared to the experimental data. One can see that the experimentally obtained and the calculated values of the skin friction agree qualitatively well.

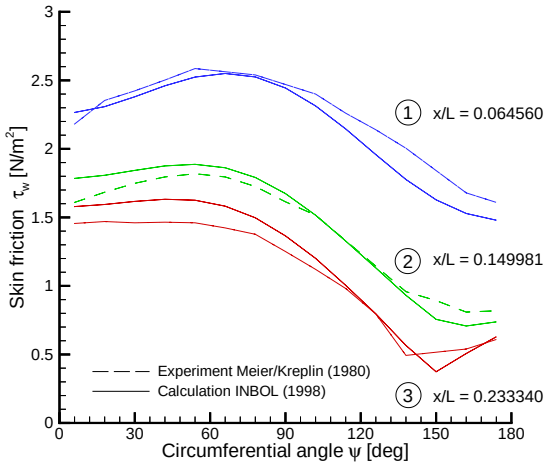

Fig. 4.5: Comparison of measured and calculated skin-friction curves for an ellipsoid of revolution 6:1 ($\alpha = 10°$, $Re_L = 7.2 \cdot 10^6$)

Results for the Hull of 'Lotte'

Results of the three-dimensional boundary-layer calculation for 'Lotte' are presented in Fig. 4.6 and Fig. 4.7. Fig. 4.6 shows the wall streamlines of 'Lotte' for an angle of attack of $\alpha = 10°$. One observes the convergence of the wall streamlines, starting at 50% of the hull length. This corresponds to the region where the shear layer starts separating from the airship body. The convergence of the limiting streamlines and the associated separation can also be seen in the experiment with turbulent flow (see section 3.2). The visualised separation topology looks more complex than the calculated separation line. So far, the 3D-method is unable to cover all separation effects.

Fig. 4.7 shows the skin-friction plotted against the circumferential angle Ψ at selected axial positions. The values of curves 1, 2, and 3 are taken from the region with attached flow. Curve 4 represents quantities for the area of beginning flow separation. It can be seen that the minimum of the shear stress lies in the vicinity of separation at approximately $\Psi = 130°$.

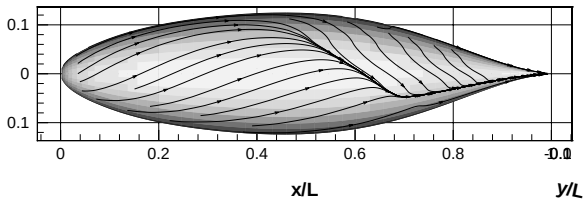

Fig. 4.6: Calculated wall streamlines for the hull of 'Lotte'
($\alpha = 10°$, $Re_L = 1.5 \cdot 10^6$)

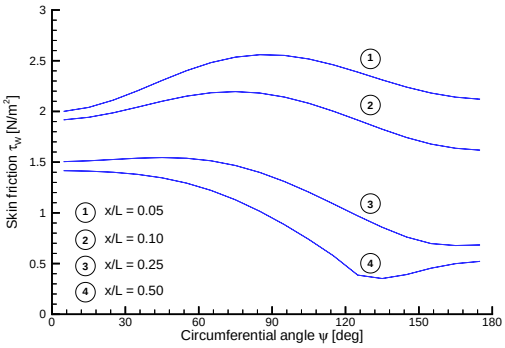

Fig. 4.7: Calculated skin-friction curves for the hull of 'Lotte'
($\alpha = 10°$, $Re_L = 1.5 \cdot 10^6$)

5 Conclusions

The phenomena of the flow about inclined airship hulls have been discussed with special consideration of three-dimensional separation effects. Flow visualisations performed in a water tunnel supplied information on the flow condition close to the wall and the topology of the separating boundary layer. Theoretical investigations on the flow field of inclined hulls were performed using a simplified calculation method. To capture three-dimensional viscous effects and to predict the shear-layer separation-line, a 3D-boundary-layer method has been developed.

A detailed interpretation of the surface flow pattern concerning separation topology as well as their quantitative analysis is part of future work. Presently, the 3D-method is being extended to calculate turbulent boundary-layers. Furthermore, the coupling of the panel method, the wake model and the 3D-method is intended.

6 References

[1] Hessenberger, K.: *Programmierung eines Integralverfahrens zur Berechnung dreidimensionaler, laminarer, kompressibler Grenzschichten;* Diplomarbeit am Institut für Aerodynamik und Gasdynamik, Universität Stuttgart (1993)

[2] Hoerner, S.F.: *Fluid Dynamic Lift;* published by the author (1979)

[3] Jones, S.P. and DeLaurier, J.D.: *Aerodynamic Estimation Techniques for Aerostats and Airships;* J. Aircraft, Vol. 20, No. 2 (1983)

[4] Lutz, Th.; Schmidt, E. and Wagner, S.: *An Efficient Calculation Method for the Determination of Force and Moment Coefficients on a Body with Boundary Layer Separation under Various Onset Flow Conditions;* Proc. of the International Airship Conference, Stuttgart, Germany, June 24-25 (1993)

[5] Lutz, Th.; Schmidt, E.; and Wagner, S.: *Berechnung der Umströmung von Luftschiffrümpfen;* Proc. Luftschiff Kolloquium II; Lübbenau / Spreewald, Germany, May 13-14 (1994)

[6] Lutz, Th.; Leinhos, D. and Wagner, S.: *Theoretical Investigations of the Flowfield of Airships with a Stern Propeller;* International Airship Convention and Exhibition, Bedford, July 5-7 (1996)

[7] Meier, H.U. and Kreplin, H.P.: *Experimental Investigation of the Boundary Layer Transition and Separation on a Body of Revolution;* Zeitschrift für Flugwissenschaften und Weltraumforschung 4, Heft 4 (1980)

[8] Merzkirch, W.: *Techniques of Flow Visualization;* AGARDograph No. 302 (1987)

[9] Putman, W.F.; Maughmer, M.; Curtiss, Jr.H.C. and Traybar, J.J.: *Aerodynamic and hovering control of LTA vehicles;* Department of Aerospace and Mechanical Sciences, Princeton University (1977)

[10] Schwarz, G.; Schall, M.; Knauss, H.: *Windkanaluntersuchungen an einem Luftschiffmodell;* Institut für Aerodynamik und Gasdynamik, Universität Stuttgart (1993)

[11] Schwarz, G.; Schall, M.; Lutz, Th.: Unpublished windtunnel experiments; Institut für Aerodynamik und Gasdynamik, Universität Stuttgart (1993)

[12] Stock, H.W.: *Laminar Boundary Layers on Inclined Ellipsoids of Revolution;* Zeitschrift für Flugwissenschaften und Weltraumforschung 4, Heft 4 (1980)

[13] Stock, H.W. and Horton, H.P.: *Ein Integralverfahren zur Berechnung dreidimensionaler, laminarer, kompressibler, adiabater Grenzschichten;* Zeitschrift für Flugwissenschaften und Weltraumforschung, Heft 2 (1985)

[14] Tseng, W.W. and Llorens, R.E.: *Application of the panel method to airships;* AIAA Lighter-Than-Air Systems Conference, Anaheim, California, July 25-27 (1983)

[15] Wortmann, F.X.; Speth, J. F.: *Der Große Wasserkanal des Instituts für Aerodynamik und Gasdynamik;* Institut für Aerodynamik und Gasdynamik (1980)